JMEPEG (2018) 27:6479–6484
https://doi.org/10.1007/s11665-018-3775-y

1059-9495/$19.00

Stability of Phase Transformation Temperatures During Cycling of Ti-15.8Nb-4.94Al-0.06Sc Shape Memory Alloy

B. Sun, X.L. Meng, Z.Y. Gao, and W. Cai

(Submitted March 1, 2018; in revised form July 9, 2018; published online November 27, 2018)

The active ω phase formation decreases the martensitic transformation temperatures sharply and can even suppress the martensitic transformation during thermal cycling in Ti-Nb-based alloys. No ω phase is observed in the present Ti-15.8Nb-4.94Al-0.06Sc alloy when it is annealed at 650 °C for 4 h or subsequently aged at 200 and 250 °C for 2 h. The exclusion of ω phase remarkably improves the stability of phase transformation temperatures during thermal cycling. The martensitic transformation start temperature of the present alloy decreases by 30 °C but tends to be stable gradually during the 20 thermal cycles, owing to the saturation of lattice defects.

Keywords biomaterial, martensitic transformation, shape memory alloys (SMAs), thermal analysis, titanium

1. Introduction

Ti-Nb based alloys are potential candidates to develop Ni-free shape memory alloys (SMAs) because of their nontoxic elements, pronounced biocompatibility and low elastic modulus (Ref 1-5). Martensitic transformation from the disordered body-centered cubic β phase to the orthorhombic α'' martensite phase occurs in the Ti-Nb-based alloys when the alloying content is above a critical value (Ref 6, 7). Ascribing to the thermoelastic martensitic transformation, satisfactory shape memory effect (SME) and superelasticity (SE) can be obtained in Ti-Nb-based alloys (Ref 8, 9). However, one disadvantage for such alloys is the instability of martensitic transformation during thermal cycling, which severely limits their applications (Ref 10, 11). For example, in the Ti-22Nb alloy, the martensitic transformation start temperature (M_s) decreases from 147 °C (the 1st cycle) to below − 100 °C (the 2nd cycle) when it is thermally cycled from − 100 to 240 °C (Ref 11). It is generally recognized that the active ω phase formation in Ti-Nb-based alloys causes the degeneration of phase transformation temperatures. The ω phase forms readily in Ti-Nb-based alloys when they are aged in the temperature range from 100 to 600 °C (thermal ω phase) (Ref 6). Besides, the ω phase can even be formed by quenching from a high temperature, which is the so-called athermal ω phase (Ref 6). Once the ω phase forms, it decreases the martensitic transformation temperatures dramatically and even suppresses the transformation completely by changing the composition of the matrix or mechanically suppressing the martensitic transformation.

Alloying elements that can stabilize the β phase has been added to Ti-Nb alloys to suppress the formation of ω phase, and it has achieved some success. For example, in $(Ti\text{-}23Nb)_{(1-x)}$-xZr alloy, the athermal ω phase is suppressed when the Zr content is above 6% (Ref 12). In Ti-24Nb-6Zr-2Ta alloy, the thermal ω phase is suppressed when it is aged at 300 °C for 99 h (Ref 13). Besides them, Al works as the β-stabilizing element in β-Ti alloys as well, though it is categorized into the α-stabilizing elements (Ref 14). Literature (Ref 15-17) reported that the addition of Al is effective on the suppression of ω phase in Ti-Ta-, Ti-Mo- and Ti-V-based alloys. In parallel, it was reported that Sc prefers to segregate at the interface of θ' precipitates and matrix in the Al-Cu alloy with minor Sc (Ref 18). The segregation of Sc reduces the interface energy and concomitantly reduces the driving force for precipitate coarsening.

In the present study, martensitic transformation behavior of the Ti-15.8Nb-4.94Al-0.06Sc alloy during thermal cycling, along with the corresponding microstructure evolution, has been investigated. Moreover, the effect of aging temperature on the martensitic transformation, the microstructure and the hardness of such an alloy has been investigated as well.

2. Experimental

The Ti-15.8Nb-4.94Al-0.06Sc (at.%) alloy ingot was fabricated by arc-melting method, using 99.99% Ti, 99.9% Nb, 99.9% Al and an Al-1.21Sc (at.%) intermediate alloy. To ensure homogeneity, the ingot was turned around after each melting and re-melted for eight times. The as-cast ingot was homogenized at 900 °C for 2 h followed by water quenching. Specimens used in this work were cut from the ingot and sealed in a vacuum quartz tube. And then, they were annealed at 650 °C for 4 h with subsequent water quenching. Some specimens were aged at 200, 250, 300, 350 and 400 °C for 2 h after annealing. XRD measurements were taken at room temperature by Panalytical Empyrean x-ray diffractometer, using the Cu Kα radiation. DSC detections were conducted by PerkinElmer Diamond differential scanning calorimeter with the heating and cooling rate of 20 °C/min. Hardness tests were conducted on a Laizhou Huayin HVS-1000 Vickers microhardness tester, using a 500 g load and 10 s dwell time. Thin foils for TEM observations were prepared using a twin-jet

B. Sun, X.L. Meng, Z.Y. Gao, and **W. Cai**, School of Materials Science and Engineering, Harbin Institute of Technology, Harbin 150001, People's Republic of China. Contact e-mail: xlmeng@hit.edu.cn.

polisher in an electrolyte composed of 6% perchloric acid, 34% *n*-butyl alcohol and 60% methanol (vol.%) at about − 20 °C. TEM observations were performed with a JEOL 2100 electron microscope operated at 200 kV.

3. Results

Figure 1(a) shows the DSC curves of the annealed Ti-15.8Nb-4.94Al-0.06Sc alloy during 20 thermal cycles from − 120 to 200 °C. The peaks related to the forward and the reverse martensitic transformation can be detected all along the 20 thermal cycles. The transformation temperatures are plotted as the function of thermal cycle number in Fig. 1(b). It is seen that M_s and the martensitic transformation start temperature (A_f) decrease rapidly in the first five thermal cycles and tend to be stable gradually with further increasing the cycle numbers. Quite different from the Ti-22Nb alloy (Ref 11), of which M_s decreases by more than 200 °C after only one thermal cycle, M_s and A_f of the present alloy decrease by 30 and 37 °C, respectively, after 20 thermal cycles. It suggests that the stability of phase transformation temperatures is improved significantly in the present alloy.

Figure 2(a) shows the DSC curves of the Ti-15.8Nb-4.94Al-0.06Sc alloy aged at 200, 250, 300, 350 and 400 °C for 2 h. No heat peaks related to the forward and the reverse martensitic transformation are detected in the DSC curves of the specimens aged at 350 and 400 °C. It indicates that forward martensitic transformation temperatures of such specimens are lower than − 120 °C. Figure 2(b) shows the aging temperature dependence of M_s and A_f, where the martensitic transformation temperatures measured after annealing are given as the 25 °C aging values in the plot for comparison with those obtained after aging. It is seen from Fig. 2(b) that the martensitic transformation temperatures decrease with the increase in aging temperature except the 300 °C aging values.

Figure 3(a) shows the XRD profiles at room temperature of the annealed Ti-15.8Nb-4.94Al-0.06Sc alloy before and after 20 thermal cycles. Three crystalline phases, β phase, α'' martensite phase and α phase, coexist in the specimen before thermal cycles. The α phase in the present alloy forms during annealing at 650 °C, which locates at the $\alpha + \beta$ dual phase field. The α'' martensite phase and β phase coexist because the XRD measurements were taken at temperature between M_f and A_f (see Fig. 1). The phase constitution does not change in the specimen after 20 thermal cycles. It consists of β phase, α'' martensite phase and α phase as well. Figure 3(b) shows the XRD profiles at room temperature of the specimens aged at 200, 250, 300, 350 and 400 °C, respectively. Phase constitution of the specimens aged at 200, 250 and 300 °C does not change compared with the annealed specimen. However, the specimens aged at 350 and 400 °C consist of β phase and α phase. And no α'' martensite phase is detected.

TEM micrographs of the annealed Ti-15.8Nb-4.94Al-0.06Sc alloy before and after 20 thermal cycles are exhibited in Fig. 4. Figure 4(a) shows the typical morphology of α'' martensite phase, residual β phase and α phase formed during annealing in the specimen before thermal cycles, which has been identified by quite a lot of SAD studies. It is seen that the α'' martensite prefers to form in the V-shape. The two martensite variants are in $\{111\}_{\alpha''}$ type I twin relationship as indicated in Fig. 4(g). The α phase is observed to be fusiform particles with the size of about 1 μm. Figure 4(f) is the SAD pattern of β phase, which is obtained from the $[011]_\beta$ zone axis. In addition to the primary reflections of the β matrix, extra diffraction spots at the $1/2(112)_\beta$ positions are observed. These extra spots are considered to be related to α phase. The circled diffraction spot in Fig. 4(f) was used to obtain the dark-field TEM image shown in Fig. 4(b). It reveals that fine α-phase particles with the size of several nanometers form during annealing besides the coarse α-phase particles. No diffraction spots corresponding to ω phase (at the $1/3(112)_\beta$ positions) are observed in this specimen. The morphology features do not change after 20 thermal cycles. V-shaped martensite variants can still be observed embedding in the β matrix (Fig. 4c), which evidences the occurrence of martensitic transformation. In addition, a lot of dislocations are observed in the specimen after 20 thermal cycles, where the g^*-vector used to obtain the image is $[011]_\beta$ (Fig. 4d). No diffraction spots corresponding to ω phase are observed in the SAD pattern of the $[011]_\beta$ zone axis (Fig. 4h). It indicates that ω phase has not formed yet after 20 thermal cycles from − 120 to 200 °C.

Figure 5 shows the TEM images of the Ti-15.8Nb-4.94Al-0.06Sc alloy aged at 200, 250, 300, 350 and 400 °C for 2 h. For the specimens aged at 200 and 250 °C, no extra diffraction spots corresponding to ω phase are observed in the SAD patterns taken from the residual β phase (Fig. 5a and b). For the specimen aged at 300 °C, strings along the $g^* = \langle 112 \rangle_\beta$ directions are observed in the SAD pattern ($[02\bar{1}]_\beta$ zone axis), while no evident diffraction spots are observed at the $1/3(112)_\beta$ positions. It suggests that ω phase has not formed

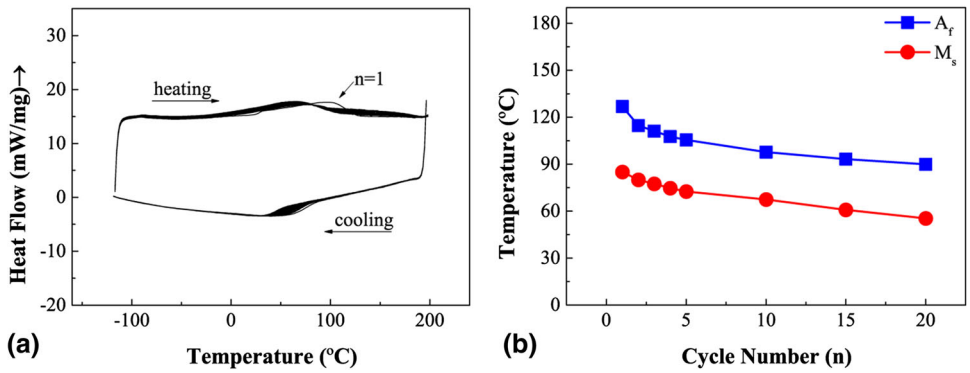

Fig. 1 (a) DSC curves of the Ti-15.8Nb-4.94Al-0.06Sc alloy during 20 thermal cycles and (b) the thermal cycling number dependence of the transformation temperatures

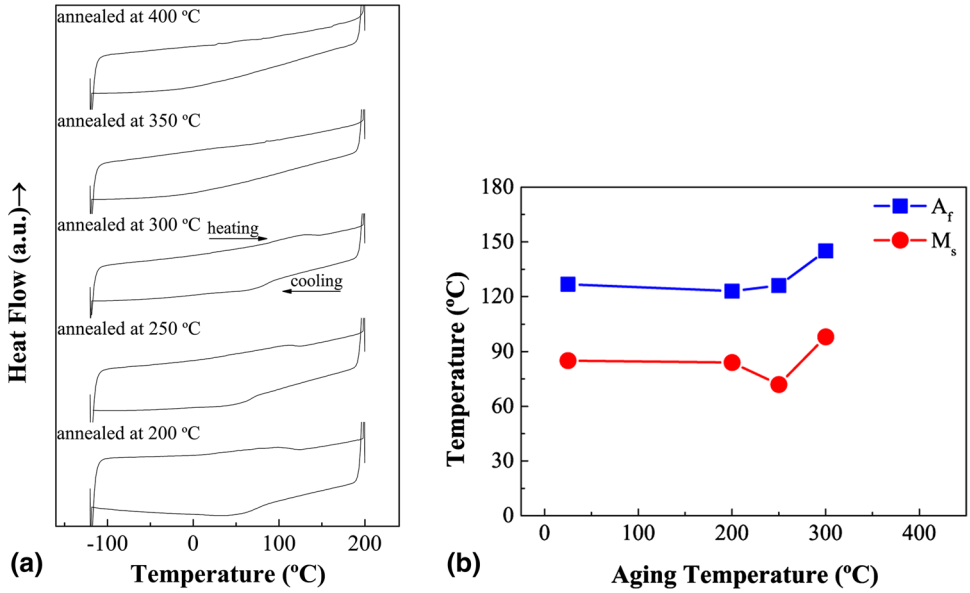

Fig. 2 (a) DSC curves of the Ti-15.8Nb-4.94Al-0.06Sc alloy aged at different temperatures for 2 h and (b) the aging temperature dependence of the transformation temperatures

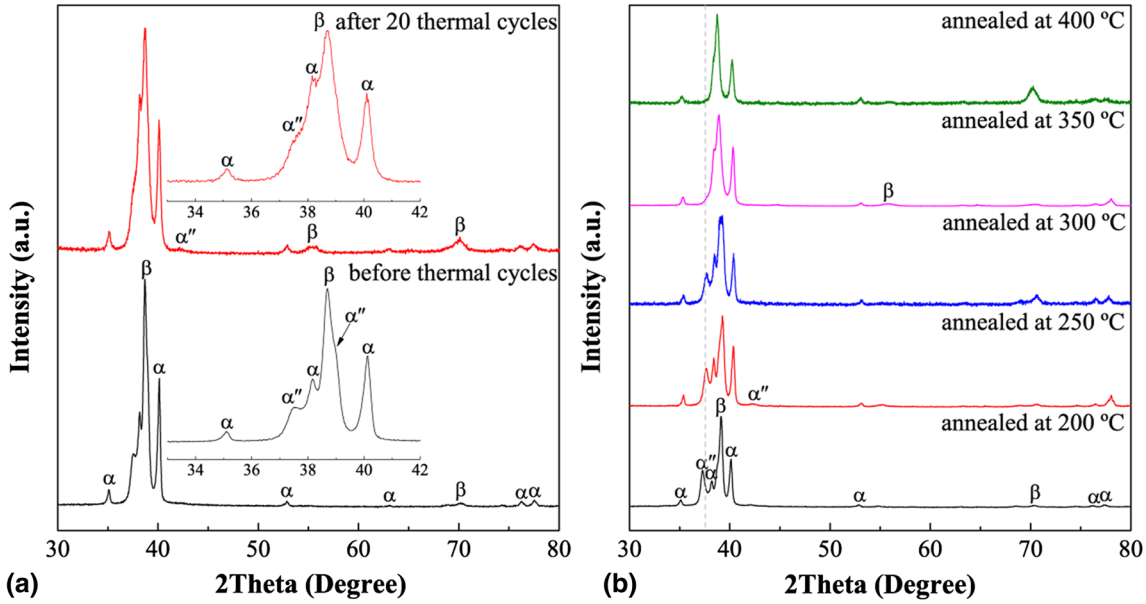

Fig. 3 XRD patterns at room temperature of the Ti-15.8Nb-4.94Al-0.06Sc alloy (a) before and after 20 thermal cycles and (b) aged at different temperatures for 2 h

yet during aging at 200, 250 and 300 °C for 2 h. The formation of ω phase has been suppressed successfully in the present Ti-15.8Nb-4.94Al-0.06Sc alloy. Diffraction spots corresponding to ω phase are observed besides those of the β phase, when the specimens are aged at 350 and 400 °C (Fig. 5d, e). The dark-field image obtained from the circled diffraction spot in Fig. 5(e) reveals the existence of plate-like ω phase in the 400 °C-aged specimen. The formation of ω phase decreases the martensitic transformation temperatures. Therefore, no diffraction peak related to α'' martensite phase is detected in the XRD measurement of such specimens.

Figure 6 shows the Vickers microhardness of the Ti-15.8Nb-4.94Al-0.06Sc alloy aged at different temperatures for 2 h. The Vickers microhardness of the annealed specimen is given as the 25 °C (room temperature) aging value in the plot for comparison with those obtained after aging. The microhardness increases monotonically while the aging temperature increases: a slow increase after aging at the low temperatures (200 and 250 °C) followed by a remarkable increase with the further increase in aging temperature. The formation of ω phase during aging is responsible for the increase in microhardness. It has been known that ω phase is beginning to form at 300 °C in

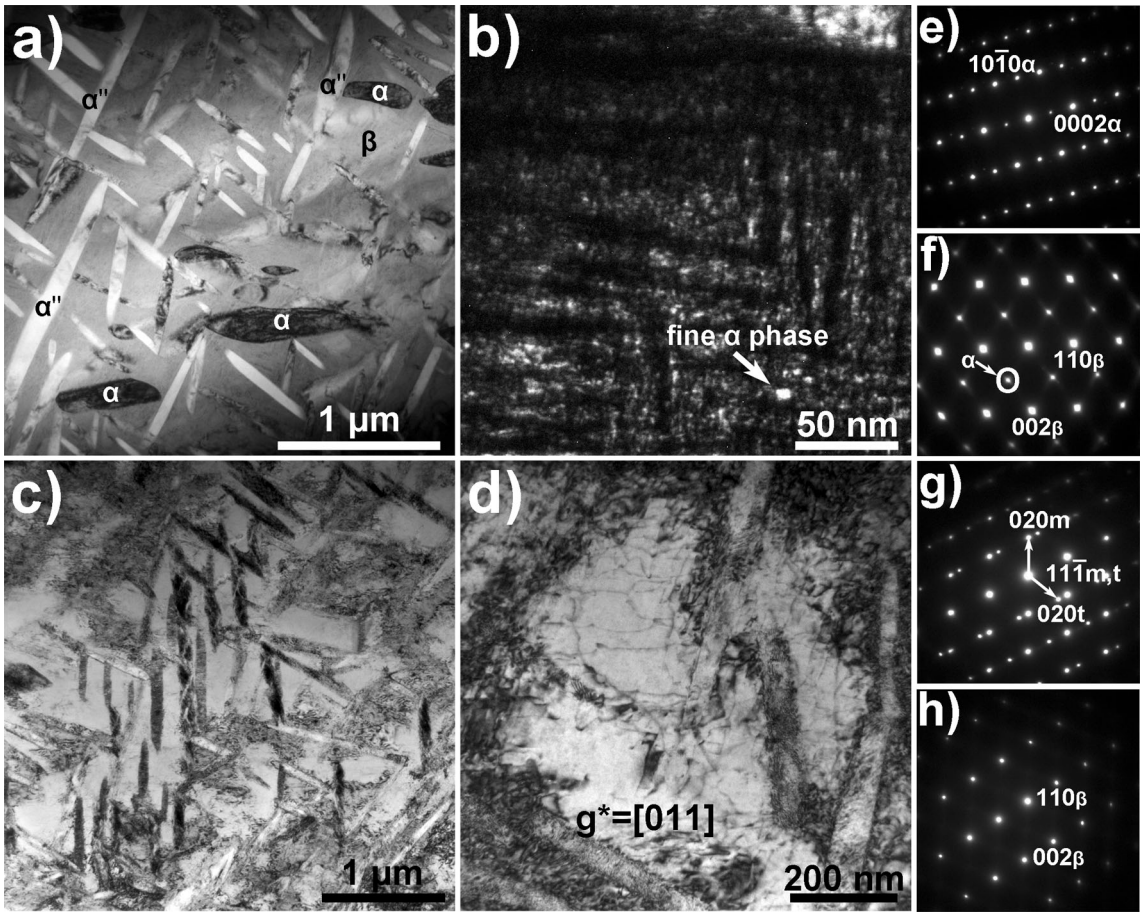

Fig. 4 TEM micrographs of the Ti-15.8Nb-4.94Al-0.06Sc alloy. (a) bright-field image before thermal cycles; (b) dark-field micrograph before thermal cycles, which is obtained from the circled diffraction spot in (f); (c), (d) bright-field images after 20 thermal cycles; (e) SAD pattern of α phase in (a); (f) SAD pattern of β matrix in (a); (g) SAD pattern taken from the interface of two martensite variants in (a) and (h) SAD pattern of β matrix in (c)

the present alloy and accordingly the microhardness increases remarkably.

4. Discussion

The exclusion of ω phase during thermal cycling is responsible for the improved stability of phase transformation temperatures. There is no ω phase observed in the specimens before thermal cycles and after 20 thermal cycles from − 120 to 200 °C. High density of tangled dislocations is observed in the specimen after 20 thermal cycles. Such lattice defects are considered to be introduced and accumulated during the repeating forward and reverse martensitic transformations. The introduction of lattice defects strengthens the β matrix. So they accumulate fast in the first few cycles, slow down as the cycle number increases and finally become saturated. The strengthening of β matrix makes the shear deformation related to the forward martensitic transformation difficult and leads to the decrease in M_s. The same rule as the accumulation of lattice defects, the M_s decreases rapidly in the first five cycles and tends to be stable gradually during the further increase in thermal cycles.

No isothermal ω phase is observed in the specimens aged at 200 and 250 °C for 2 h. And the martensitic transformation temperatures of such specimens change little compared with the annealed specimen. Evident diffraction spots corresponding to ω phase are observed in the SAD patterns taken from the specimens aged at 350 and 400 °C for 2 h. Accordingly, martensitic transformation temperatures of such specimens decrease dramatically (lower than − 120 °C).

From the above discussion, we know that the addition of Al and minor Sc is effective to suppress the formation of ω phase in the Ti-Nb-based alloys. $\overline{Bo} - \overline{Md}$ diagrams have been proved useful in the design of Ti-based alloys (Ref 12, 14). Here, $\overline{Bo}$ is the average bond order between Ti and the alloying elements, while $\overline{Md}$ is the average *d*-orbital energy level of the alloying elements. It gives the boundary for the precipitation of ω phase in the diagram according to the value of $\overline{Bo}$ and $\overline{Bo}$ of the alloys. The farther the alloy lied from such boundary, the more difficultly ω phase forms. By substituting Al ($\overline{Bo} = 2.426$, $\overline{Md} = 2.200$) to Ti ($\overline{Bo} = 2.790$, $\overline{Md} = 2.447$), the position of the alloy shifts downward in the diagram, which is a very efficient route to get away from the boundary for ω phase formation. As a result, the present Ti-15.8Nb-4.94Al-0.06Sc alloy lies much farther from this boundary than the Ti-24Nb or Ti-24Nb-0.5Si alloys. Accordingly, the formation of ω phase becomes more difficult. Compared with the Ti-24Nb-3Al alloy, where ω phase has formed already during quenching from the elevated temperature (Ref 19), ω phase forms more

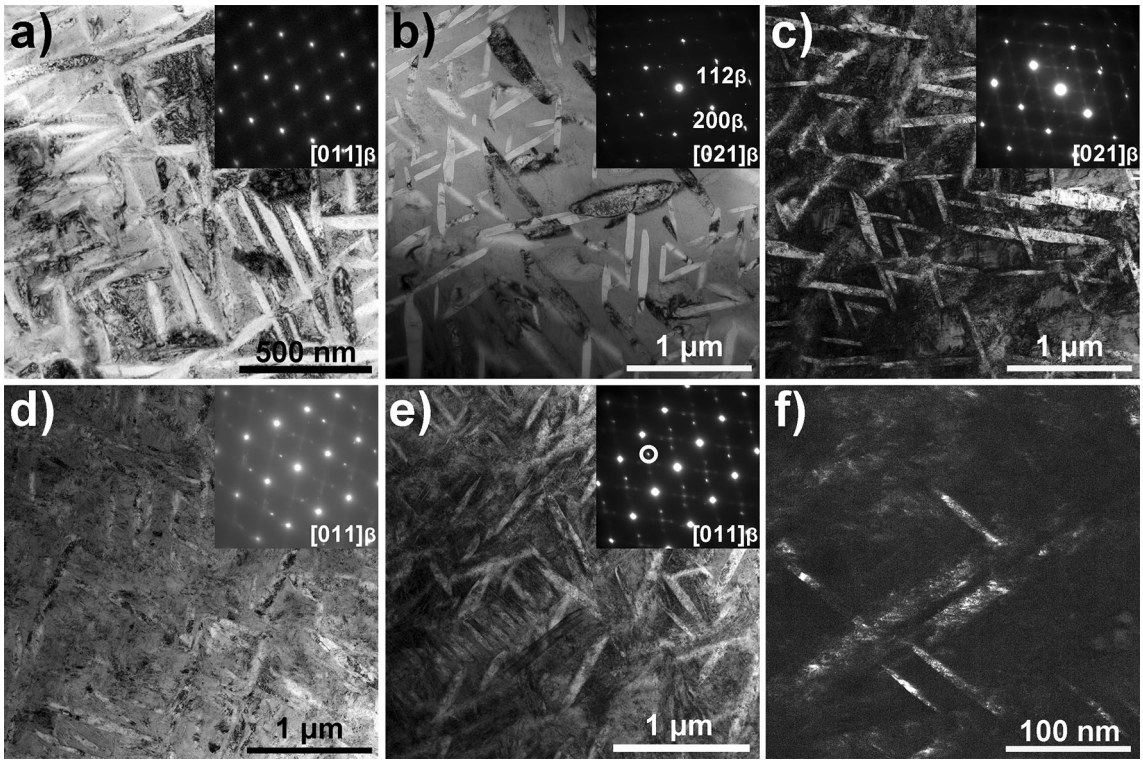

Fig. 5 TEM micrographs of the Ti-15.8Nb-4.94Al-0.06Sc alloy aged at different temperatures for 2 h. (a) to (e) bright-field images of the specimens aged at 200, 250, 300, 350 and 400°C, the corresponding SAD pattern of the β matrix is shown as an inset for each image and (f) dark-field image of the 400°C-aged specimen obtained by the circled diffraction spot in (e)

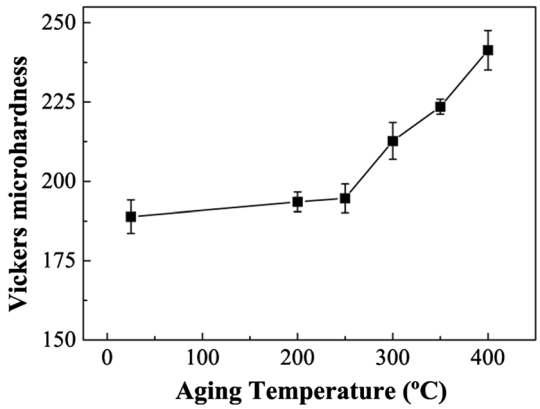

Fig. 6 The aging temperature dependence of the Vickers microhardness in the Ti-15.8Nb-4.94Al-0.06Sc alloy

difficultly in the present alloy. So it is speculated that the addition of minor Sc may also contribute to suppress the formation of ω phase.

It is noted that the transformation interval of the forward and reverse martensitic transformation is quite large in the annealed alloy. This phenomenon is in concern with the formation of fine α phase during annealing at 650 °C. The stress field around the fine α-phase particles impedes the propagation of martensite front during the growth of martensite. This stress distributes heterogeneously since the size of α-phase particles and the inter-particle distance are different. As a result, the extra driven force aroused from undercooling deviates and the transformation interval widens.

5. Conclusion

The stability of phase transformation temperatures is remarkably improved in the present Ti-15.8Nb-4.94Al-0.06Sc alloy. M_s tends to be stable gradually during the 20 thermal cycles, owing to the saturation of lattice defects. No ω phase is observed in the specimens before thermal cycle, after 20 thermal cycles from − 120 to 200 °C and aged at the low temperatures (200 and 250 °C) for 2 h. It indicates that the addition of Al and minor Sc is able to suppress the formation of ω phase. The exclusion of ω phase is responsible for the improved stability of phase transformation temperatures during thermal cycling.

Acknowledgments

The work was supported by National Natural Science Foundation of China (No. 51571073) and State Key Lab of Advanced Metals and Materials (2015-Z01).

References

1. Y.W. Chai, H.Y. Kim, H. Hosoda, and S. Miyazaki, Self-accommodation in Ti-Nb Shape Memory Alloys, *Acta Mater.*, 2009, **57**, p 4054–4064
2. Y.W. Chai, H.Y. Kim, H. Hosoda, and S. Miyazaki, Interfacial Defects in Ti-Nb Shape Memory Alloys, *Acta Mater.*, 2008, **56**, p 3088–3097
3. Y.F. Zheng, B.L. Wang, J.G. Wang, C. Li, and L.C. Zhao, Corrosion Behaviour of Ti-Nb-Sn Shape Memory Alloys in Different Simulated Body Solutions, *Mater. Sci. Eng. A*, 2006, **438-440**, p 891–895

4. C.R.M. Afonso, G.T. Aleixo, A.J. Ramirez, and R. Caram, Influence of Cooling Rate on Microstructure of Ti-Nb Alloy for Orthopedic Implants, *Mater. Sci. Eng. C*, 2007, **27**, p 908–913
5. S. Dubinskiy, V. Brailovski, S. Prokoshkin, V. Pushin, K. Inaekyan, V. Sheremetyev, M. Petrzhik, and M. Filonov, Structure and Properties of Ti-19.7Nb-5.8Ta Shape Memory Alloy Subjected to Thermomechanical Processing Including Aging, *J. Mater. Eng. Perform.*, 2013, **22**, p 2656–2664
6. H.Y. Kim, Y. Ikehara, J.I. Kim, H. Hosoda, and S. Miyazaki, Martensitic Transformation, Shape Memory Effect and Superelasticity of Ti-Nb Binary Alloys, *Acta Mater.*, 2006, **54**, p 2419–2429
7. T. Ahmed and H.J. Rack, Martensitic Transformations in Ti-(16-26 at.%) Nb Alloys, *J. Mater. Sci.*, 1996, **31**, p 4267–4276
8. B. Sun, X.L. Meng, Z.Y. Gao, W. Cai, and L.C. Zhao, Effect of Annealing Temperature on Shape Memory Effect of Cold-rolled Ti-16 at.% Nb Alloy, *J. Alloys Compd.*, 2017, **715**, p 16–20
9. F. Sun, S. Nowak, T. Gloriant, P. Laheurte, A. Eberhardt, and F. Prima, Influence of a Short Thermal Treatment on the Superelastic Properties of a Titanium-based Alloy, *Scr. Mater.*, 2010, **63**, p 1053–1056
10. P.J.S. Buenconsejo, H.Y. Kim, H. Hosoda, and S. Miyazaki, Shape Memory Behavior of Ti-Ta and its Potential as a High-temperature Shape Memory Alloy, *Acta Mater.*, 2009, **57**, p 1068–1077
11. A. Ramalohary, P. Castany, P. Laheurte, F. Prima, and T. Gloriant, Superelastic Property Induced by Low-temperature Heating of a Shape Memory Ti-24Nb-0.5Si Biomedical Alloy, *Scr. Mater.*, 2014, **88**, p 25–28
12. M. Abdel-Hady, H. Fuwa, K. Hinoshita, H. Kimura, Y. Shinzato, and M. Morinaga, Phase Stability Change with Zr Content in β-type Ti-Nb Alloys, *Scr. Mater.*, 2007, **57**, p 1000–1003
13. P.L. Ferrandini, F.F. Cardoso, S.A. Souza, C.R. Afonso, and R. Caram, Aging Response of the Ti-35Nb-7Zr-5Ta and Ti-35Nb-7Ta Alloys, *J. Alloys Compd.*, 2007, **433**, p 207–210
14. M. Abdel-Hady, K. Hinoshita, and M. Morinaga, General Approach to Phase Stability and Elastic Properties of β-type Ti-alloys Using Electronic Parameters, *Scr. Mater.*, 2006, **55**, p 477–480
15. P.J.S. Buenconsejo, H.Y. Kim, and S. Miyazaki, Effect of Ternary Alloying Elements on the Shape Memory Behavior of Ti-Ta Alloys, *Acta Mater.*, 2009, **57**, p 2509–2515
16. J.C. Williams, B.S. Hickman, and D.H. Leslie, The Effect of Ternary Additions on the Decompositon of Metastable Beta-Phase Titanium Alloys, *Metall. Trans.*, 1971, **2**, p 477–484
17. G.H. Narayanan and T.F. Archbold, Decomposition of the Metastable Beta Phase in the All-Beta Alloy Ti-13 V-11Cr-3Al, *Metall. Trans.*, 1970, **1**, p 2281–2290
18. C. Yang, P. Zhang, D. Shao, R.H. Wang, L.F. Cao, J.Y. Zhang, G. Liu, B.A. Chen, and J. Sun, The Influence of Sc Solute Partitioning on the Microalloying Effect and Mechanical Properties of Al-Cu Alloys with Minor Sc Addition, *Acta Mater.*, 2016, **119**, p 68–79
19. T. Inamura, Y. Fukui, H. Hosoda, K. Wakashima, and S. Miyazaki, Mechanical Properties of a Ti-Nb-Al Shape Memory Alloy, *Mater. Trans.*, 2004, **45**, p 1083–1089